Polymer Chemistry

ROYAL SOCIETY OF CHEMISTRY

PAPER

View Article Online
View Journal | View Issue

Cite this: *Polym. Chem.*, 2023, **14**, 662

A systematic study of a polymer-assisted carboxylate-based MOF synthesis: multiple roles of core cross-linked PMAA-*b*-PMMA nanoparticles†

Mingyuan Fang,[a] Didier Cot,[a] Carmen Montoro*[a,b] and Mona Semsarilar *[a]

Carboxylate-based metal organic frameworks (MOFs) coordinated by multiple-functional carboxylic acid linkers and various metals represent a large family of MOFs. Carboxylic acid functionalized polymers, such as poly(acrylic acid), polystyrene-*b*-(acrylic acid) and poly(methacrylic acid)-*co*-(ethylene glycol di-methacrylate), have been used in the synthesis of carboxylate-based MOFs in order to modulate, or provide a template for, the growth of MOF crystals. Although this strategy has been used to prepare MOFs, the role of the carboxylic acid functionalized (co)polymers in the synthesis of MOFs is still not very clear. In this article, we report the synthesis of UiO-66 (a MOF designed at the University of Oslo) in the presence of core cross-linked poly(methacrylic acid)-*b*-poly(methyl methacrylate) (PMAA-*b*-PMMA) nanoparticles (NPs), with two different modulators (acetic acid (HAc) and hydrochloric acid (HCl)) and in the absence of any modulator. Additionally, a series of reactions were carried out where the classical terephthalic acid (TA) linker was replaced with PMAA-*b*-PMMA NPs. These experiments elucidated the role of NPs in the polymer-assisted synthesis as well as how the PMAA-*b*-PMMA NPs become incorporated into the final UiO–polymer hybrid investigated material. In this polymer-assisted UiO-MOF synthesis, the PMAA-*b*-PMMA NPs act as a stabilizer, a template and a (co)modulator to form the final UiO–polymer hybrid NPs with different colloidal aspects, sizes and crystallinity.

Received 20th September 2022,
Accepted 30th December 2022

DOI: 10.1039/d2py01202b

rsc.li/polymers

1. Introduction

Metal organic frameworks (MOFs) are crystalline and porous materials constructed by the coordination bonds between metal ions or clusters and organic linkers.[1] They are characterized by large surface areas with tunable pore sizes and high thermal and chemical stabilities, which make them good candidates for many applications, such as gas capture and separation, catalysis, sensing and pollutant removal.[2–6]

One of the most representative MOF families is that of carboxylate-based MOFs, formed by the union between multiple-functional carboxylic acid linkers and various metals.[1] The use of carboxylic acid functionalized polymers during their synthesis allows us to modulate, or provide a template for, the growth of MOF crystals. In this sense, Lotsch *et al.*[7] used poly (acrylic acid) (PAA) to control the particle size of HKUST-1 (a MOF first synthesized at the Hong Kong University of Science and Technology). PAA was also used to synthesize UiO-66 (a MOF designed at the University of Oslo) with narrow particle size distributions.[8] Moreover, block-copolymers with a carboxylic chain were also used as templates for preparing mesoporous MOFs. For example, polystyrene-*b*-(acrylic acid) oligomers and poly(methacrylic acid)-*co*-(ethylene glycol dimethacrylate) were used as soft templates for the preparation of mesoporous HKUST-1.[9,10] Although this strategy has been used to prepare carboxylate-based MOFs, the role of carboxylic acid functionalized polymers, especially block copolymers with carboxylic acid functions, in MOF synthesis is still not very clear.

Previously, we have described the successful synthesis of stable UiO–polymer NPs using spherical core cross-linked poly (methacrylic acid)-*b*-poly(methyl methacrylate) (PMAA-*b*-PMMA) nanoparticles (NPs) *via* a reversible addition–fragmentation chain-transfer polymerization controlled polymerization induced self-assembly (RAFT-PISA) method.[11] The exceptional colloidal stability of this material facilitated the preparation of a thin-film membrane ideal for nanofiltration. In this case, in order to further delve into the mechanism of the formation of

[a]*Institut Européen des Membranes—IEM UMR 5635, Université Montpellier, CNRS, ENSCM, 34095 Montpellier, France. E-mail: carmen.montoro@uam.es, mona.semsarilar@umontpellier.fr*
[b]*Departamento de Química Inorgánica, Universidad Autónoma de Madrid, 28049 Madrid, Spain*

† Electronic supplementary information (ESI) available. See DOI: https://doi.org/10.1039/d2py01202b

UiO MOFs with core cross-linked PMAA-*b*-PMMA NPs, we have designed the synthesis of UiO-66 in the presence of different sizes of core cross-linked PMAA-*b*-PMMA NPs, two different modulators (acetic acid (HAc) and hydrochloric acid (HCl)) and in the absence of any modulator. HAc and HCl have been proved as efficient modulators for UiO synthesis.[12,13] The use of HAc leads to the formation of large crystals. In contrast, the use of HCl as a modulator allows the reaction to take place at a lower temperature with a high reaction rate, which is advantageous due to the presence of polymers (reducing the risk of polymer degradation at higher temperatures). Other carboxylic acid modulators have also been applied in MOF synthesis, such as benzoic acid,[12] formic acid and propionic acid.[14] Moreover, the impact of different mono-functional carboxylic acid modulators on the sizes of particles and their colloidal stability was also further studied.[15] Here, we investigate the role of PMAA-*b*-PMMA NPs in the formation of UiO–polymer hybrids as compared to the classical UiO-66. In addition, the possibility of using these NPs as modulators was also studied where no extra modulator was added to the synthesis media. In addition, to further study the role of PMAA-*b*-PMMA NPs in the process of UiO synthesis, a series of reactions were designed where the H_2BDC linker (1,4-benzenedicarboxylic acid, terephthalic acid, TA) was gradually replaced with PMAA-*b*-PMMA NPs while keeping the same number of moles of acid functionality in the synthesis system (with zero H_2BDC linker and 100% PMAA-*b*-PMMA NPs). The carboxylic acid functionalities provided strong coordination sites for the Zr ions/clusters. By gradually replacing the classical UiO-66 linker with PMAA-*b*-PMMA NPs, the influence of the NPs and how they become integrated in the final UiO–polymer hybrid material were studied.

2. Materials and methods

2.1. Materials

Methacrylic acid (MAA) (4-methoxyphenol, MEHQ used as an inhibitor; 99.0%), 4-cyano-4-(phenylcarbonothioylthio)pentanoic acid (>97.0%), 4,4-azobis(4-cyanovaleric acid) (ACVA; 98.0%), methyl methacrylate (MMA) (MEHQ used as an inhibitor, 99.0%), 2,2′-azobis(2-methylpropionitrile) (AIBN; 98.0%), ethylene glycol dimethacrylate (EGDMA) (MEHQ used as an inhibitor; 98%), (trimethylsilyl)diazomethane solution 2.0 M in diethyl ether, zirconium(IV) chloride ($ZrCl_4$; ≥99.5% trace metals basis), acetic acid (HAc; ≥99%) and hydrochloric acid (HCl, 37%) were purchased from Sigma-Aldrich while terephthalic acid (TA; ≥98.0%) was purchased from Alpha Aesar. Solvents were purchased from Fisher Scientific and VWR. All reagents were used without further purification.

2.2. Methods

2.2.1. Synthesis of poly(methacrylic acid) (PMAA). $PMAA_{64}$, used as the macro chain transfer agent ($PMAA_{64}$ mCTA), was synthesized following our previously reported procedure.[11] MAA (12 g, 135.3 mmol), 4-cyano-4-(phenylcarbonothioylthio) pentanoic acid (540.8 mg, 1.93 mmol), targeting a molecular degree of polymerisation (DP) of 70, and ACVA (54.26 mg, 0.19 mmol; CTA/ACVA molar ratio = 10) were dissolved in ethanol (12 g). The reaction mixture was placed under nitrogen and heated at 70 °C for 6 h (≥99% monomer conversion). The polymerization was quenched by cooling the reaction mixture and exposing it to air. Finally, the reaction mixture was diluted with a two-fold excess of ethanol. The resulting solid was dried under vacuum for 24 h and a targeted mean degree of polymerization (DP) of 64 was established using ^{1}H NMR spectroscopy (Fig. S1a†).

2.2.2. Synthesis of poly(methacrylic acid)-*b*-poly(methyl methacrylate) (PMAA-*b*-PMMA) nanoparticles (NPs). PMAA-*b*-PMMA NPs at 20% w/w in ethanol were prepared *via* the RAFT-PISA method, following a similar procedure previously reported by us.[11] Briefly, MMA (1 g, 10 mmol), AIBN initiator (1.8 mg, 0.01 mmol), and $PMAA_{64}$ macro-CTA (200 mg, 0.036 mmol) were dissolved in ethanol (7 g). The reaction mixture was sealed in a 10 mL round bottom flask, purged with N_2 for 10 min and kept at 70 °C until ^{1}H NMR analysis showed an MMA conversion of 90% (about 33 h, see Fig. S1b†). Then, the PMAA-*b*-PMMA NPs were cross-linked by the addition of 10 mol% (to MMA) EGDMA. The reaction was carried out at 70 °C for a further 12 h and a pink viscous solution (gel-like) in ethanol was obtained.

PMAA-*b*-PMMA powder was collected after centrifugation at 4400 rpm (2460 RCF) for 40 minutes. The pink gel obtained was first dried in air for 4 hours and then dried under vacuum for 8 hours.

2.2.3. Synthesis of UiO-66 using HAc (UiO-66-HAc) and HCl (UiO-66-HCl) as modulators. UiO-66-HAc was synthesized using a similar method previously reported by Behrens *et al.*[12] employing 0.5 mL of acetic acid as the modulator (see details in Table S1†).

UiO-66-HCl was synthesized following a previous report with some modifications (see details in Table S1†).[12] $ZrCl_4$ (0.25 mmol, 58.3 mg) and TA (0.25 mmol, 41.5 mg) were dissolved separately in 4 mL of *N*,*N*-dimethylformamide (DMF) by sonication for about 10 minutes. After mixing these two solutions, 0.4 mL of HCl (1.4 molar ratio to $ZrCl_4$) was added to the mixture. The final mixture was sonicated for 2 minutes and then transferred to a 20 mL glass pressure tube that was heated at 80 °C. After 12 hours, a white precipitate of UiO-66-HCl in DMF was obtained. To isolate the powder, the reaction mixture was centrifuged at 4400 rpm for 5 minutes. The washing and centrifugation cycles were repeated using DMF (2 × 10 mL) and then with ethanol (3 × 10 mL). The resulting white powder was dried under vacuum at 80 °C for 8 hours.

2.2.4. Synthesis of UiO–polymer hybrid NPs using HAc (UiO-P-20%-HAc) and HCl as modulators (UiO-P-20%-HCl) or without using a modulator (UiO-P-20%-No modulator). UiO-P-20%-HAc NPs were prepared following the same method previously reported by us.[11]

For the preparation of UiO-P-20%-HCl NPs, in the first step, PMAA-*b*-PMMA NPs 20% w/w in ethanol (20% molar ratio of carboxylic acid function of PMAA-*b*-PMMA to zirconium; see

details in Table S1†) were dispersed in 2 mL of DMF and stirred for 1 hour. $ZrCl_4$ (0.25 mmol, 58.3 mg) was dissolved in 3 mL of DMF by sonication for about 10 minutes and mixed with the PMAA-*b*-PMMA NPs DMF dispersion for about 5 minutes using sonication. TA (0.25 mmol, 41.5 mg) was also dissolved in 3 mL of DMF and then 0.4 mL of HCl (1.4 molar ratio to $ZrCl_4$) was also added to the mixture of polymer NPs and $ZrCl_4$. The final mixture was sonicated for 2 minutes and then transferred to a 20 mL cylindrical glass pressure vessel that was heated at 80 °C. After 12 hours, a light pink viscous solution (gel-like) of UiO–polymer NPs in DMF was obtained. To isolate the dry powder, the viscous solution was centrifuged at 4400 rpm for 20 minutes. The washing and centrifugation cycles were repeated using DMF (2 × 10 mL) and then with ethanol (3 × 10 mL). The resulting white powder was dried under vacuum at 80 °C for 8 hours.

The synthesis of UiO-P-20%-No modulator NPs was carried out following the same formulation as in UiO-P-20%-HAc (see details in Table S1†). The initial mixture without acetic acid was heated at 120 °C for 20 h and a light pink viscous solution in DMF was obtained. To isolate the dry powder, the solution was centrifuged at 4400 rpm for 40 minutes. The washing and centrifugation cycles were repeated using DMF (2 × 10 mL) and then with ethanol (3 × 10 mL). The light pink powder was dried under vacuum at 80 °C for 8 hours.

2.2.5. Study of TA replacement by PMAA-*b*-PMMA NPs in UiO-66 synthesis. UiO-66-TA_1 was prepared following the same procedure as UiO-66-HCl (see details in Table S2†). Then, UiO-TA_X-P_Y materials were prepared following the synthesis conditions explained for UiO-P-20%-HCl. Briefly, the TA was gradually replaced with PMAA-*b*-PMMA NPs to maintain the same number of moles of acid function in the reaction mixture ($X + Y = 1$) until no TA and 100% of PMAA-*b*-PMMA NPs were achieved (see details in Table S2†). The resulting product of UiO-$TA_{0.9}$-$P_{0.1}$ was a light pink solution, UiO-$TA_{0.8}$-$P_{0.2}$ and UiO-$TA_{0.5}$-$P_{0.5}$ were a light pink viscous solution (gel-like) and UiO-TA_0-P_1 was a pink transparent viscous solution (gel-like). To isolate the dry powders, the reaction mixtures were centrifuged at 4400 rpm for 10 minutes to 1 hour depending on their different viscosity and colloidal stability. The washing and centrifugation cycles were repeated using DMF (2 × 10 mL) and then using ethanol (3 × 10 mL). The white or pink powders were dried under vacuum at 80 °C for 8 hours.

2.3. Characterization studies

^{1}H NMR spectra were recorded on a 400 MHz Bruker Avance spectrometer. PMAA-*b*-PMMA molecular weight and distributions were determined using size exclusion chromatography (SEC) with a double detector array from Viscotek (TDA 305, Malvern Instruments, Worcestershire, UK). The Viscotek SEC apparatus was equipped with a two-column set-up with a common particle size of 5 mm and a refractive index detector (RI, concentration detector). Tetrahydrofuran (THF) was used as an eluent (1.0 mL min^{-1}) and polystyrene was used as the standard (15 standard samples ranging from 100 to 1 000 000 g mol^{-1}) for number average molecular weights (M_n) and the dispersity index ($Đ$). OmniSEC software was used for data acquisition and analysis. For SEC, PMAA and PMAA-*b*-PMMA were modified by methylation of the carboxylic acid groups on the polymer chain using an excess of trimethylsilyldiazomethane. Briefly, 20 mg of the PMAA or PMAA-*b*-PMMA was dissolved in THF and trimethylsilyldiazomethane (yellow solution) was added dropwise at room temperature. The addition of trimethylsilyldiazomethane was continued until the colorless solution turned yellow. A few drops of trimethylsilyldiazomethane were added and the solution was stirred overnight to make sure the methylation was complete. Centrifugation of colloidal solutions was performed using a Sigma Laboratory centrifuge (using 4400 rpm–2460 RCF (g)). Powder X-ray diffraction (XRD) was carried out on a PANalytical X'pert Pro diffractometer with reflectance parallel beam/parallel slit alignment geometry. The measurement employed Cu Kα line focused radiation at 800 W (40 kV, 20 mA) power. Samples were observed using a 0.017° 2θ step scan from 5° to 50° with a 120 s exposure time per step. The powder diffraction pattern was calculated based on previously published crystal data[16] *via* VESTA software. Fourier-transform infrared (FT-IR) spectra were recorded on a Thermo Nicolet iS50 FT-IR spectrometer in transmission mode. Sample pellets were prepared with 1 mg of sample grinded and pressed with 200 mg of KBr powder. Each pellet was subjected to 32 scans from 400 cm^{-1} to 4000 cm^{-1}. Scanning electron microscopy (SEM) images were obtained from a Hitachi S4800 with a working voltage ranging from 0.1 to 30 kV. Transmission electron microscopy (TEM) images were obtained from a JEOL 1200 EXII (or JEOL 1400 Flash) under working voltages up to 120 kV. TEM samples were prepared by dropping 10 μL of the sample (previously diluted 50 times from the reaction mixture and stirred for at least 1 hour to ensure a homogeneous dispersion) on a carbon-coated copper TEM grid and left for 1 minute. The PMAA-*b*-PMMA samples were stained for 20 s using ammonium molybdate. Then the grid was dried for 1 minute using a vacuum hose under ambient conditions. All the image analyses were performed using ImageJ software. Nitrogen adsorption isotherms were measured at 77 K on a Micromeritics ASAP 2020 Plus Adsorption Analyzer. Prior to measurement, powder samples were degassed for 12 h at 373 K.

3. Results and discussion

The core cross-linked $PMAA_{64}$-*b*-$PMMA_{254}$ NPs were synthesized in ethanol *via* RAFT-mediated PISA, following our previously reported procedure.[10] In brief, a well-defined PMAA macro-CTA with a mean DP of 64 (M_n = 14.3 kg mol^{-1}, M_w = 14.9 kg mol^{-1}, $Đ$ = 1.04) was block extended with MMA in ethanol under dispersion PISA conditions. The conversion of MMA was followed by ^{1}H NMR (Fig. S1b†). The resulting $PMAA_{64}$-*b*-$PMMA_{254}$ NPs (M_n = 24.5 kg mol^{-1}, $Đ$ = 1.28) were core cross-linked *via* the addition of EGDMA. The cross-linking

Table 1 Nanoparticle size and morphology obtained using TEM and SEM images

Material	Size (nm) by TEM	Size (nm) by SEM	Shape
PMAA-*b*-PMMA	45–80	NA	Spherical[a]
	90–265	NA	Short worm[a]
	45–90	NA	Spherical[b]
	105–300	NA	Short worm[b]
UiO-P-20%-HAc	100–200	80–150	Spherical
UiO-P-20%-No modulator	NA	60–90	Spherical
UiO-P-20%-HCl	50–80	50–80	Spherical
UiO-66-HCl	NA	70–300	Spherical (inter-grown)
UiO-66-HAc	NA	6000	Octahedral

[a] Core cross-linked $PMAA_{64}$-*b*-$PMMA_{254}$ NPs dispersed in ethanol. [b] Core cross-linked $PMAA_{64}$-*b*-$PMMA_{254}$ NPs dispersed in DMF.

of the core would prevent the NPs from solubilizing in organic solvents.

The size and shape of PMAA-*b*-PMMA NPs were analyzed by TEM and SEM (Table 1). The TEM results showed that the diameter of the PMAA-*b*-PMMA NPs before cross-linking in ethanol was 45–65 nm for individual spherical NPs. These spherical NPs had a tendency to form dimers and trimers (short worms) (Fig. S2a†). These short worms had a length range of 100 to 220 nm. After cross-linking with EGDMA, the morphologies were maintained but the sizes were slightly larger than the NPs before the cross-linking. In particular, the sizes calculated from TEM images were 45–80 nm for individual spherical NPs (Fig. S2b†), and the lengths were 90 to 265 nm for the short worms in ethanol (Fig. S2b†). Then, NPs were dispersed in DMF, preserving their morphology (Fig. S2c†). Since DMF is a good solvent for both polymer blocks, the NPs swelled to a larger diameter of 45–90 nm. So, the TEM images indicated the preservation of the shape and size of the core cross-linked PMAA-*b*-PMMA NPs in ethanol and DMF.

Then, the core cross-linked PMAA-*b*-PMMA NPs were used in the synthesis of UiO–polymer NPs (Scheme 1). Previously, we have demonstrated that the presence of 20 mol% of PMAA-*b*-PMMA spherical NPs in the synthesis of UiO-66 would give a better control over the homogeneity and colloidal stability of the MOF–polymer hybrid material in DMF.[10] Thus, this optimal ratio of 20% was maintained in this study and the synthetic conditions were modified through the presence of a modulator such as HAc or HCl or without a modulator. Again, the size and shape of UiO–polymer NPs obtained from different modulation syntheses (UiO-P-20%-HAc, UiO-P-20%-HCl and UiO-P-20%-no modulator) were analyzed by SEM and TEM (Table 1) and the results compared with the pristine material obtained following the same modulation conditions but without using polymer NPs (UiO-66-HAc and UiO-66-HCl). The SEM image of UiO-P-20%-HAc NPs (Fig. 1a) shows a spherical shape with sharp edges and the particle sizes ranged from 100 to 200 nm. Compared to the UiO-66-HAc crystals (Fig. S3†), the particle shape changed from octahedral to spherical and particle sizes became much smaller. TEM images of UiO-P-20%-HAc NPs (Fig. S4a†) confirmed the spherical shape with sharp edges and sizes comparable to the results from SEM. It should be emphasized that only a few particles could be observed due to the high viscosity of the solution, which were difficult to disperse and dilute for the TEM analysis.

On the other hand, the solution of UiO-P-20%-HAc NPs in DMF showed a colloidal stability of about 7 days. The viscosity aspect of this solution was due to the presence of the PMAA-*b*-PMMA NPs forming short worms (since they can entangle and increase the viscosity of the NP solution[17,18]). These short worms will provide a smaller number of accessible acid functionalities and lower particle mobility in solution as compared to spherical nanoparticles. The larger NP size and fewer accessible acid functionalities led to the formation of different particle sizes and physical behavior of the final UiO–polymer hybrid NPs indicating that the morphology of the used PMAA-*b*-PMMA NPs has a marked influence on the properties of the hybrid material (larger particles, broader size distribution and lower colloidal stability).

In the case of the synthesis of UiO-66 in the presence of core cross-linked PMAA-*b*-PMMA NPs and without a modulator (UiO-P-20%-No modulator), the resulting NPs also formed a pink viscous solution in DMF with good colloidal stability. These NPs were spherical and small (50 to 90 nm by SEM).

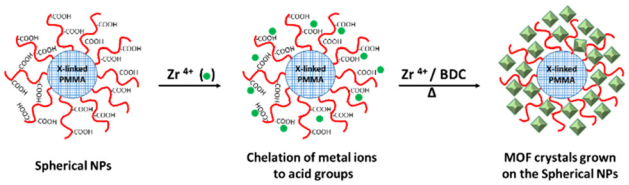

Scheme 1 Synthesis of UiO-66 crystals initiated from the surface of core cross-linked PMAA-*b*-PMMA spherical NPs.

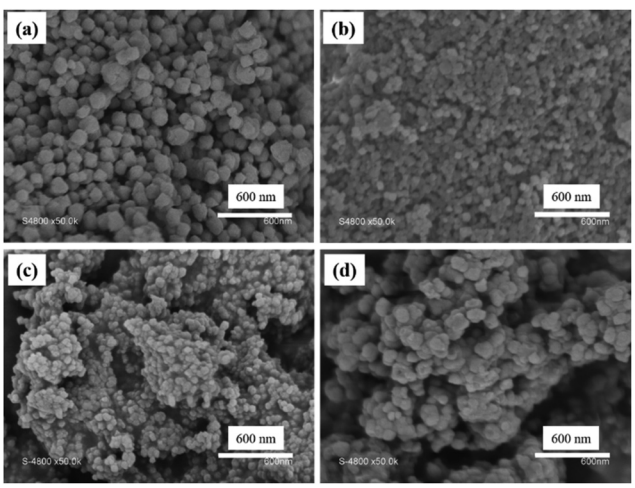

Fig. 1 SEM images of (a) UiO-P-20%-HAc, (b) UiO-P-20%-No modulator, (c) UiO-P-20%-HCl and (d) UiO-66-HCl.

This size is very close to the size of the PMAA-*b*-PMMA NPs (Fig. 1b). Since the PMAA-*b*-PMMA NPs have multiple carboxylic acid functions on their surface, the Zr ions and clusters can coordinate with these acid functions. Then, UiO-66 will preferentially grow from the surface of the PMAA-*b*-PMMA NPs where the Zr content is higher. If there are modulators in the system, the modulator (for example, HAc) could form intermediate complexes with Zr ions and favor the further growth of UiO crystals.[12] In the absence of a modulator, the UiO crystals will grow from each Zr coordinated to the PMAA-*b*-PMMA NPs resulting in the final NPs (UiO-P-20%-No modulator) with almost the same size as that of the PMAA-*b*-PMMA NPs. The small particle size and the limited UiO growth on the PMAA-*b*-PMMA NPs made the UiO-P-20%-No modulator NPs a more stable colloid in DMF. In this case, the PMAA-*b*-PMMA NPs act both as the modulator and as the template for the growth of UiO crystals. There are also some large aggregates with a size range from 200 to 500 nm and no defined shape. These aggregates are very similar to the dried polymer particles.

PMAA-*b*-PMMA NPs in the HCl-modulated UiO–polymer synthesis acted the same as in the case of HAc-modulated synthesis, forming a stable viscous solution of UiO NPs in DMF. The resulting UiO-P-20%-HCl showed spherical NPs with a size 50–80 nm under SEM (Fig. 1c). The spherical shape and similar size of UiO-P-20%-HCl NPs were confirmed by TEM. Spherical UiO-P-20%-HCl particles were connected together *via* the polymer due to the high viscosity (Fig. S4b†), while the UiO-66-HCl sample presented inter-grown spherical NPs from 70 to 300 nm as seen in the SEM image (Fig. 1d).

In the two examples where HAc and HCl were used as modulators, the particle size of the final UiO–polymer hybrid NPs was smaller than the UiO synthesized under the same conditions but in the absence of PMAA-*b*-PMMA NPs. In a classical MOF synthesis using a mono-functional modulator (such as HCl or HAc), metal ions would form an intermediate complex with the mono-functional modulator and favor the growth of a few large UiO crystals *via* exchanging the metal from the complex with the di-functional linker. But in the case of the assisted synthesis with PMAA-*b*-PMMA NPs, the metal ions would coordinate with the PMAA-*b*-PMMA NPs in a homogeneous manner. This would lead to the preferential growth of the UiO crystals from the surface of PMAA-*b*-PMMA NPs, which allows for the formation of smaller but more homogeneous UiO NPs.

Structural characterization of UiO-P-20%-HAc, UiO-P-20%-No modulator and UiO-P-20%-HCl was carried out using XRD (Fig. 2). All the main peaks of pristine UiO-66 (HAc and HCl) were present in the diffraction patterns of UiO–polymer hybrids (UiO-P-20%-HAc, UiO-P-20%-No modulator, UiO-P-20%-HCl), confirming the formation of the same crystalline structure. This means that the presence of PMAA-*b*-PMMA NPs does not affect the crystalline growth phase of the pristine UiO-66.

The hybrid UiO–polymer NPs were further analyzed using FT-IR measurements (Fig. 3). It was noted that the characteristic C=O stretching of the uncoordinated carboxylate group

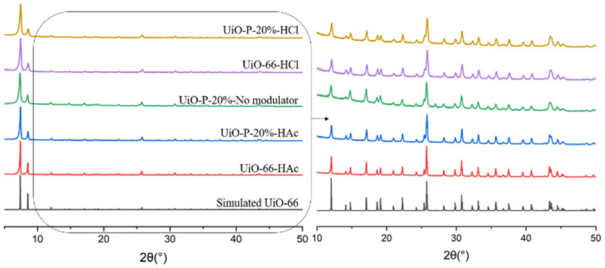

Fig. 2 XRD patterns of simulated UiO-66,[16] UiO-66-HAc, UiO-P-20%-HAc, UiO-P-20%-No modulator, UiO-P-20%-HCl and UiO-66-HCl.

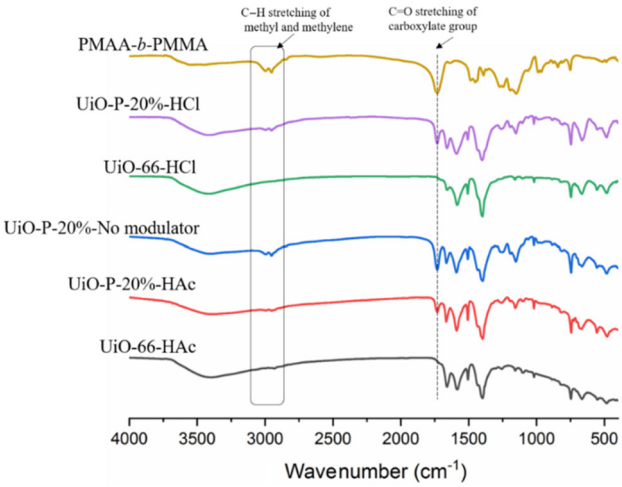

Fig. 3 FT-IR spectrum of UiO-66-HAc, UiO-P-20%-HAc, UiO-P-20%-No modulator, UiO-P-20%-HCl, UiO-66-HCl and PMAA-*b*-PMMA NPs.

at 1730 cm^{-1} and C–H stretching of methyl and methylene groups between 2995 and 2955 cm^{-1} from PMAA-*b*-PMMA NPs appeared in all three UiO–polymer hybrid samples (UiO-P-20%-HAc, UiO-P-20%-No modulator, UiO-P-20%-HCl), indicating that the PMAA-*b*-PMMA NPs were successfully incorporated into the UiO–polymer hybrid structure.

To conclude, in a preformed polymer-assisted UiO synthesis, the shape and morphology of the PMAA-*b*-PMMA NPs have a strong impact on the final UiO–polymer hybrid colloidal behavior (stable colloid solution or viscous solution) and particle homogeneity. For example, small spherical PMAA-*b*-PMMA NPs lead to a stable colloidal solution with homogeneous UiO–polymer hybrid NPs.[10] In contrast, larger spherical or short worm-like PMAA-*b*-PMMA NPs result in the formation of a viscous solution and wider size range of hybrid NPs. PMAA-*b*-PMMA NPs could also act as modulators themselves or as a co-modulator with a mono-functional acid (HAc or HCl) to synthesize UiO–polymer hybrid NPs with small size and good crystallinity.

With an aim of understanding how the PMAA-*b*-PMMA NPs interact with Zr ions/clusters and integrate into the final UiO–polymer hybrid structure, a series of reactions were performed where the UiO-66 linker (TA) was gradually replaced with

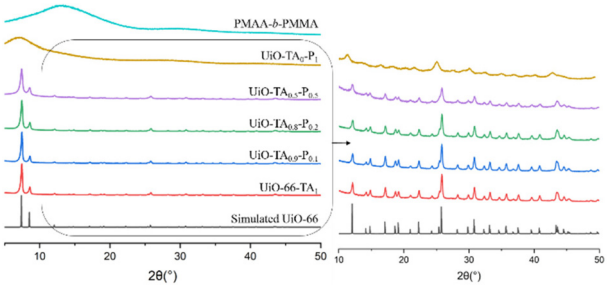

Fig. 4 XRD patterns of simulated UiO-66,[16] UiO-66-TA_1, UiO-$TA_{0.9}$-$P_{0.1}$, UiO-$TA_{0.8}$-$P_{0.2}$, UiO-$TA_{0.5}$-$P_{0.5}$, UiO-TA_0-P_1, and PMAA-*b*-PMMA.

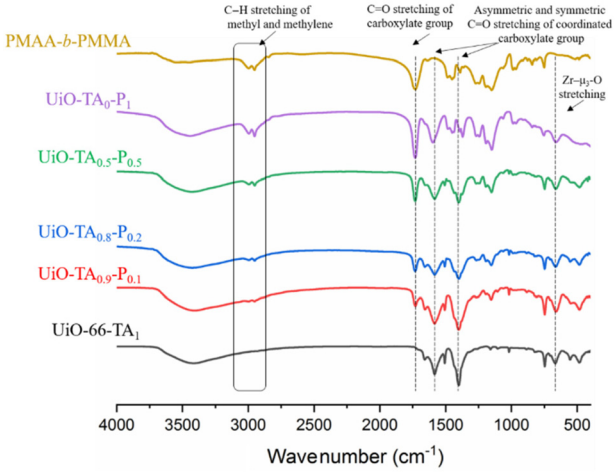

Fig. 5 FT-IR spectrum of UiO-66-TA_1, UiO-$TA_{0.9}$-$P_{0.1}$, UiO-$TA_{0.8}$-$P_{0.2}$, UiO-$TA_{0.5}$-$P_{0.5}$, UiO-TA_0-P_1, and PMAA-*b*-PMMA.

PMAA-*b*-PMMA NPs. For this, a series of UiO–polymer hybrids with increasing polymer content were synthesized (UiO-$TA_{0.9}$-$P_{0.1}$, UiO-$TA_{0.8}$-$P_{0.2}$ and UiO-$TA_{0.5}$-$P_{0.5}$). In the absence of the linker, a Zr-coordinated polymer network was obtained (UiO-TA_0-P_1). The interactions between Zr ions or clusters with the acid groups on the PMAA-*b*-PMMA NPs lead to the formation of an amorphous network as shown in the XRD and FT-IR results.

The XRD patterns (Fig. 4) of UiO-$TA_{0.9}$-$P_{0.1}$ and UiO-$TA_{0.8}$-$P_{0.2}$ showed intense diffraction peaks, as expected. The small amount of missing TA linker maybe partially replaced by the acid functionalities on the PMAA-*b*-PMMA NPs or created some linker defects in the UiO–polymer structure. Nonetheless, the whole structure remained highly crystalline. The UiO–polymer synthesized with only 50 mol% of the linker, UiO-$TA_{0.5}$-$P_{0.5}$, was still crystalline. All the diffraction peaks of UiO-66 from 5° to 50° (2θ) could be found in the UiO-$TA_{0.5}$-$P_{0.5}$ with broader signals and reduced intensity indicating the decrease of crystallinity. UiO-TA_0-P_1 synthesized with only the PMAA-*b*-PMMA NPs and $ZrCl_4$ led to a non-crystalline material with a broad signal starting from 5° to 12° (2θ), which is different from the non-coordinated PMAA-*b*-PMMA NPs.

The UiO–polymer hybrid materials with different ratios of TA and PMAA-*b*-PMMA were further analyzed by FT-IR (Fig. 5). It was noted that the characteristic C=O stretching of the uncoordinated carboxylate group at 1730 cm^{-1} and C–H stretching of the methyl and methylene groups between 2995 and 2955 cm^{-1} from PMAA-*b*-PMMA NPs appeared from UiO-$TA_{0.9}$-$P_{0.1}$ to UiO-$TA_{0.5}$-$P_{0.5}$ samples with increased intensity. All characterization peaks of UiO-66 were found in the spectra of UiO-$TA_{0.9}$-$P_{0.1}$ to UiO-$TA_{0.5}$-$P_{0.5}$ samples. These further confirmed that same chemical bonding of hybrid samples (UiO-$TA_{0.9}$-$P_{0.1}$ to UiO-$TA_{0.5}$-$P_{0.5}$) with UiO-66 and quantity of integrated PMAA-*b*-PMMA NPs increased. For UiO-TA_0-P_1, two bands at 1600 cm^{-1} (initially at 1585 cm^{-1} in UiO-66) and 1401 cm^{-1} are assigned to the asymmetric and symmetric stretching vibrations of the coordinated carboxylate C=O group, respectively. A broad band at 660 cm^{-1} was also found in the UiO-TA_0-P_1 spectrum, which is at the same wavenumber as that of Zr–μ_3-O bonding in UiO-66, indicating that the coordination of Zr–O between metal and PMAA-*b*-PMMA NPs is similar to that of Zr–μ_3-O bonding.[19] These signals affirmed new coordination bonds formed between the PMAA-*b*-PMMA NPs and Zr resulting in the formation of a metal-coordinated polymer network.

Nitrogen adsorption isotherms (Fig. 6) of the pristine UiO-66 exhibit a typical type I isotherm at 77 K with a Brunauer–Emmett–Teller (BET) surface area of 1177 $m^2\ g^{-1}$, indicating the uniform microporous structure of UiO-66-TA_1. Then, by gradually replacing the linker, UiO-$TA_{0.9}$-$P_{0.1}$, UiO-$TA_{0.8}$-$P_{0.2}$ and UiO-$TA_{0.5}$-$P_{0.5}$ showed mixed type I and type IV isotherms with BET surface areas of 920 and 392 $m^2\ g^{-1}$, respectively. As was expected, the replacement of linker reduced the adsorption capacity of the micropores ($P/P_0 < 0.1$) and at the same time opened the mesopores due to linker defects and the introduction of polymer NPs. The desorption

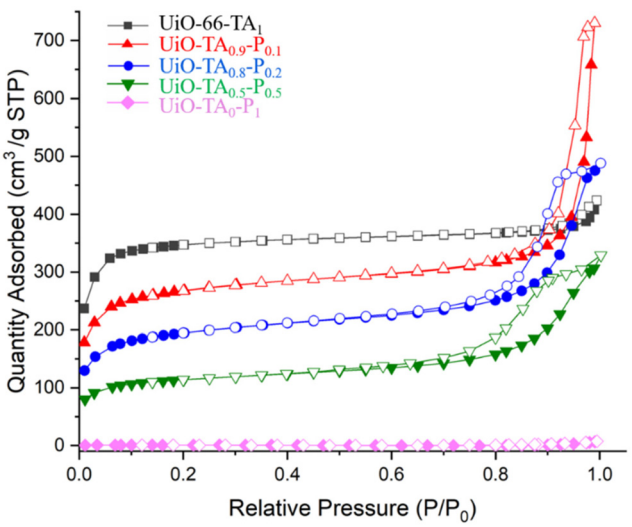

Fig. 6 N_2 adsorption isotherms measured at 77 K for UiO-66-TA_1, UiO-$TA_{0.9}$-$P_{0.1}$, UiO-$TA_{0.8}$-$P_{0.2}$, UiO-$TA_{0.5}$-$P_{0.5}$, and UiO-TA_0-P_1. Filled and empty symbols represent adsorption and desorption, respectively.

hysteresis from 0.6 to 1 (P/P_0) increased gradually from UiO-$TA_{0.9}$-$P_{0.1}$ to UiO-$TA_{0.5}$-$P_{0.5}$, which may indicate the increasing of mesoporous areas by the replacement of the linker (Fig. S6†), although sometimes such hysteresis loops can also be found for microporous MOFs. This also highlights that including up to 50% polymer NPs in the synthesis media still leads to the formation of a porous MOF–polymer structure. UiO-TA_0-P_1 showed a surface area of only 1.8 m^2 g^{-1} at 77 K since the polymer network would collapse at this temperature.

SEM images of these UiO–polymer hybrids showed that particle size became smaller when the ratio of PMAA-*b*-PMMA increased. UiO-$TA_{0.9}$-$P_{0.1}$ presented spherical NPs with sizes from 50 to 90 nm and few inter-grown crystals (Fig. 7a). The TEM image of UiO-$TA_{0.9}$-$P_{0.1}$ showed spherical particles with the same size as observed from SEM (Fig. S5a†). UiO-$TA_{0.8}$-$P_{0.2}$ showed spherical NPs with a smaller size from 30 to 50 nm (Fig. 7b). UiO-$TA_{0.5}$-$P_{0.5}$ NPs had a size of 30 to 40 nm with connected particles (Fig. 7c). The same connecting aspect was also observed under TEM, where UiO-$TA_{0.5}$-$P_{0.5}$ NPs were connected and partially covered with the polymer (Fig. S5b†). There are also some small particles (<10 nm) visible in the TEM image of UiO-$TA_{0.5}$-$P_{0.5}$ (Fig. S5b†). This could be Zr ions coordinated to the acid groups on the surface of the PMAA-*b*-PMMA NPs. UiO-TA_0-P_1 (Fig. 7d) showed a porous morphology with some particles that were very similar to the PMAA-*b*-PMMA NPs. The morphology of this sample is very different from the initial PMAA-*b*-PMMA NPs after drying (Fig. S7†). The PMAA-*b*-PMMA NPs after drying form a dense agglomerate block, while the UiO-TA_0-P_1 forms a porous light powder. This may be due to the network formed *via* Zr coordination with PMAA-*b*-PMMA NPs, preventing structural collapse during the drying step.

This set of data showed that in the presence of up to 50 mol% of PMAA-*b*-PMMA NPs, crystalline and porous UiO–polymer hybrid material could be formed with properties comparable to the UiO-66 structure. In addition, when only the PMAA-*b*-PMMA NPs were used (no TA: UiO-TA_0-P_1), the Zr ions coordinated with the acid groups on the surface of the polymer NPs forming a metal-coordinated polymer network. This network could be considered as the starting point of the UiO-66 growth in the presence of acid-functionalized polymer-assisted MOF synthesis.

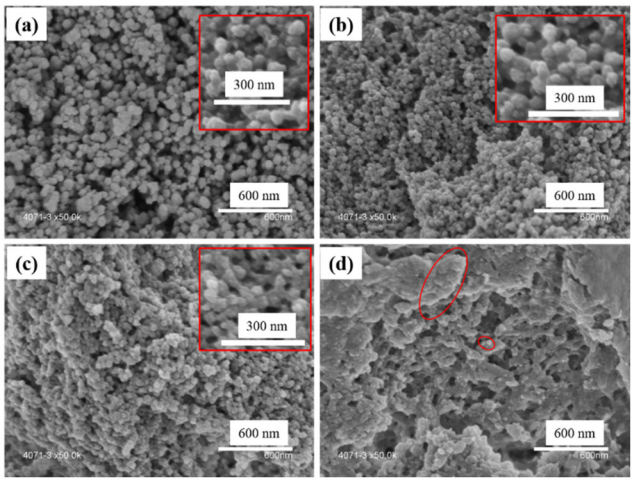

Fig. 7 SEM images of (a) UiO-$TA_{0.9}$-$P_{0.1}$, (b) UiO-$TA_{0.8}$-$P_{0.2}$, (c) UiO-$TA_{0.5}$-$P_{0.5}$, and (d) UiO-TA_0-P_1.

4. Conclusions

An in-depth study was carried out to investigate how the UiO-66 framework would grow in the presence of PMAA-*b*-PMMA NPs that would lead to the formation of hybrid MOF–polymer NPs. The first set of experiments revealed that a stable colloid of hybrid NPs could be synthesized regardless of the original morphology of the polymer NPs used. Furthermore, it was shown that by using polymer NPs of different morphologies (spheres (reported in our previous work[11]) *vs.* short worms), the viscosity of the final MOF–polymer hybrid NPs could be controlled (from stable colloid solution to viscous solution). This is an important finding, as control over the viscosity of the NP solution is an important issue in materials processing (for example, in the preparation of coatings, thin films, porous foams, *etc.*). Since the outer layer (shell) of the polymer NPs was covered with acid groups (polymethacrylic acid (PMAA)), the role of these acid moieties in the formation of the hybrid NPs was investigated. By varying the type of modulator (HCl, HAc, polymer NPs), it was demonstrated that when a monoacid modulator was used, larger MOF particles were generated as would be in the case of classical UiO-66 synthesis. In contrast, in the absence of monoacids and only the polymer NPs (polyacid groups), smaller MOF particles were generated. The presence of polymer NPs also leads to the formation of homogeneous MOF-containing solutions. The presence of PMAA-*b*-PMMA NPs provided strong coordination sites for Zr and good interaction with the solvent due to the soluble PMAA chains. Hence, it seems that polymer NPs have a dual role in the formation of hybrid NPs: (i) as an anchoring point for the metal ions (a template for the growth of the MOFs) and (ii) a modulator (polyacid). In addition, when the molar ratio between polymer NPs and the classical UiO-66 linker (TA) was varied, no change was observed in the crystal pattern of the generated UiO-66, confirming that the polymer NPs do not take part in forming the crystal structure but act only as a template/guide (surface for the initiation) for the growth of the MOF structure. Naturally, a minimum percentage of the classical linker (TA) is required in order to form a porous network. Again, this finding highlights the robustness of this approach in producing hybrid NPs with varied properties that could be dialed-in depending on the final application.

Conflicts of interest

There are no conflicts to declare.

Acknowledgements

MF acknowledges the financial support of the China Scholarship Council (CSC), grant number 201708070001. Institut Carnot is also acknowledged for supporting this project (16 CARN 0008-01). The INC-CNRS is thanked for the post-doctoral fellowship of CM. Mathias Gravelle is thanked for his help with experimental setups.

References

1 N. Stock and S. Biswas, *Chem. Rev.*, 2012, **112**, 933–969.
2 Q. Qian, P. A. Asinger, M. J. Lee, G. Han, K. Mizrahi Rodriguez, S. Lin, F. M. Benedetti, A. X. Wu, W. S. Chi and Z. P. Smith, *Chem. Rev.*, 2020, **120**, 8161–8266.
3 A. Kirchon, L. Feng, H. F. Drake, E. A. Joseph and H. C. Zhou, *Chem. Soc. Rev.*, 2018, **47**, 8611–8638.
4 C. Wang, X. Liu, N. K. Demir, J. P. Chen and K. Li, *Chem. Soc. Rev.*, 2016, **45**, 5107–5134.
5 Y. Bai, Y. Dou, L. H. Xie, W. Rutledge, J. R. Li and H. C. Zhou, *Chem. Soc. Rev.*, 2016, **45**, 2327–2367.
6 K. Dashtian, S. Shahbazi, M. Tayebi and Z. Masoumi, *Coord. Chem. Rev.*, 2021, **445**, 214097.
7 A. Ranft, S. B. Betzler, F. Haase and B. V. Lotsch, *CrystEngComm*, 2013, **15**, 9296–9300.
8 K. C. Bentz, S. Ayala, M. Kalaj and S. M. Cohen, *Aust. J. Chem.*, 2019, **72**, 848–851.
9 S. Cao, G. Gody, W. Zhao, S. Perrier, X. Peng, C. Ducati, D. Zhao and A. K. Cheetham, *Chem. Sci.*, 2013, **4**, 3573–3577.
10 H. Martínez-Pérez-Cejuela, M. Guiñez, E. F. Simó-Alfonso, P. Amorós, J. El Haskouri and J. M. Herrero-Martínez, *Microchim. Acta*, 2020, **187**, 1–9.
11 M. Fang, J. Cambedouzou, D. Cot, C. Montoro and M. Semsarilar, *J. Membr. Sci.*, 2022, **657**, 120669.
12 A. Schaate, P. Roy, A. Godt, J. Lippke, F. Waltz, M. Wiebcke and P. Behrens, *Chem. – Eur. J.*, 2011, **17**, 6643–6651.
13 M. J. Katz, Z. J. Brown, Y. J. Colón, P. W. Siu, K. A. Scheidt, R. Q. Snurr, J. T. Hupp and O. K. Farha, *Chem. Commun.*, 2013, **49**, 9449–9451.
14 G. Zahn, H. A. Schulze, J. Lippke, S. König, U. Sazama, M. Fröba and P. Behrens, *Microporous Mesoporous Mater.*, 2015, **203**, 186–194.
15 W. Morris, S. Wang, D. Cho, E. Auyeung, P. Li, O. K. Farha and C. A. Mirkin, *ACS Appl. Mater. Interfaces*, 2017, **9**, 33413–33418.
16 S. Øien, D. Wragg, H. Reinsch, S. Svelle, S. Bordiga, C. Lamberti and K. P. Lillerud, *Cryst. Growth Des.*, 2014, **14**, 5370–5372.
17 M. Semsarilar, E. R. Jones, A. Blanazs and S. P. Armes, *Adv. Mater.*, 2012, **24**, 3378–3382.
18 L. Upadhyaya, M. Semsarilar, R. Fernández-Pacheco, G. Martinez, R. Mallada, A. Deratani and D. Quemener, *Polym. Chem.*, 2016, **7**, 1899–1906.
19 T. T. Li, Y. M. Liu, T. Wang, Y. L. Wu, Y. L. He, R. Yang and S. R. Zheng, *Microporous Mesoporous Mater.*, 2018, **272**, 101–108.